Research Article | Vol. 24, No. 20 | 3 Oct 2016 | OPTICS EXPRESS 22528

Optics EXPRESS

Holography with a neutron interferometer

Dusan Sarenac,[1,2,*] Michael G. Huber,[3] Benjamin Heacock,[4,5] Muhammad Arif,[3] Charles W. Clark,[3,6] David G. Cory,[2,7,8,9] Chandra B. Shahi,[6,10] and Dmitry A. Pushin[1,2]

[1] *Department of Physics, University of Waterloo, Waterloo, ON, N2L3G1, Canada*
[2] *Institute for Quantum Computing, University of Waterloo, Waterloo, ON, N2L3G1, Canada*
[3] *National Institute of Standards and Technology, Gaithersburg, MD 20899, USA*
[4] *North Carolina State University, Raleigh, North Carolina 27695, USA*
[5] *Triangle Universities Nuclear Laboratory, Durham, North Carolina 27708, USA*
[6] *Joint Quantum Institute, College Park, MD 20742, USA*
[7] *Department of Chemistry, University of Waterloo, Waterloo, ON, N2L3G1, Canada*
[8] *Perimeter Institute for Theoretical Physics, Waterloo, ON, N2L2Y5, Canada*
[9] *Canadian Institute for Advanced Research, Toronto, Ontario, M5G 1Z8, Canada*
[10] *Physics and Engineering Physics Department, Tulane University, New Orleans, LA 70188, USA*
[*] *dsarenac@uwaterloo.ca*

Abstract: We use a Mach-Zehnder interferometer to perform neutron holography of a spiral phase plate. The object beam passes through a spiral phase plate, acquiring the phase twist characteristic of orbital angular momentum states. The reference beam passes through a fused silica prism, acquiring a linear phase gradient. The resulting hologram is a fork dislocation image, which could be used to reconstruct neutron beams with various orbital angular momenta. This work paves the way for novel applications of neutron holography, diffraction and imaging.

OCIS codes: (050.4865) Optical vortices; (090.1995) Digital holography; (120.3180) Interferometry; (350.5500) Propagation.

References and links

1. D. Gabor, "A new microscopic principle," Nature **161**, 777–778 (1948).
2. U. Schnars and W. P. O. Jüptner, "Digital recording and numerical reconstruction of holograms," Meas. Sci. Technol. **13**, R85-R101 (2002).
3. H. Lichte and M. Lehmann, "Electron holography–basics and applications," Rep. Prog. Phys. **71**, 016102 (2008).
4. B. Sur, R. B. Rogge, R. P. Hammond, V. N. P. Anghel and J. Katsaras,"Atomic structure holography using thermal neutrons," Nature **414**, 525–527 (2001).
5. L. Cser, Gy. Török, G. Krexner, I. Sharkov and and B. Faragó, "Holographic Imaging of Atoms Using Thermal Neutrons," Phys. Rev. Lett. **89**, 175504 (2002).
6. I. S. Anderson, R. McGreevy and H. Z. Bilheux, eds., *Neutron Imaging and Applications: A Reference for the Imaging Community* (Springer US, 2009).
7. E. N. Leith and J. Upatnieks, "Reconstructed wavefronts and communication theory," J. Opt. Soc. Am. **52**(10), 1123–1130 (1962).
8. E. N. Leith and J. Upatnieks, "Wavefront reconstruction with continuous-tone objects," J. Opt. Soc. Am. **53**(12), 1377–1381 (1963).
9. B. Javidi, ed. *Optical and Digital Techniques for Information Security* (Springer Science & Business Media, 2005).
10. S. F. Johnston *Holograms: A Cultural History* (Oxford University, 2016).
11. P. Hessing, B. Pfau, E. Guehrs, M. Schneider, L. Shemilt, J. Geilhufe, and S. Eisebitt, "Holography-guided ptychography with soft X-rays," Opt. Express **24**, 1840–1851 (2016).
12. O. Backoach, S. Kariv, P. Girshovitz, and N. T. Shaked, "Fast phase processing in off-axis holography by CUDA including parallel phase unwrapping," Opt. Express **24**, 3177–3188 (2016).
13. R. Isogai, Y. Nakamura, H. Takagi, T. Goto, P. B. Lim, and M. Inoue, "Thermomagnetic writing into magnetophotonic microcavities controlling thermal diffusion for volumetric magnetic holography," Opt. Express **24**, 522–527 (2016).
14. T. C. Petersen, A. I. Bishop, S. A. Eastwood, D. M. Paganin, K. S. Morgan, and M. J. Morgan, "Singularimetry of local phase gradients using vortex lattices and in-line holography," Opt. Express **24**, 2259–2272 (2016).
15. P. Zolliker and E. Hack, "THz holography in reflection using a high resolution microbolometer array," Opt. Express **23**, 10957–10967 (2015).
16. M. R. Fernández-Ruiz, L. Lei, M. Rochette, and J. Azaña, "All-optical wavelength conversion based on time-domain holography," Opt. Express **23**, 22847–22856 (2015).

#268545 http://dx.doi.org/10.1364/OE.24.022528
Journal © 2016 Received 16 Jun 2016; revised 8 Sep 2016; accepted 9 Sep 2016; published 20 Sep 2016

Optics EXPRESS

17. D. Bowman, P. Ireland, G. D. Bruce, and D. Cassettari, "Multi-wavelength holography with a single spatial light modulator for ultracold atom experiments," Opt. Express **23**, 8365–8372 (2015).
18. H. Rauch and S. A. Werner, *Neutron Interferometry: Lessons in Experimental Quantum Mechanics, Wave-Particle Duality, and Entanglement* (Oxford University, 2015).
19. C. W. Clark, R. Barankov, M. G. Huber, M. Arif, D. G. Cory, and D. A. Pushin, "Controlling neutron orbital angular momentum," Nature **525**, 504–506 (2015).
20. V. Y. Bazhenov, M. V. Vasnetsov and M. S. Soskin, "Laser beams with screw dislocations in their wavefronts," Pis'ma Zh. Eks. Teor. Fiz. **52**, 1037–1039 (1990) [JETP Lett. **52**, 429–431 (1991)].
21. N. R. Heckenberg, R. McDuff, C. P. Smith, and A. G. White, "Generation of optical phase singularities by computer-generated holograms," Opt. Lett. **17** 221–223 (1992).
22. H. He, N. R. Heckenberg, and H. Rubinsztein-Dunlop, "Optical particle trapping with higher-order doughnut beams produced using high efficiency computer generated holograms," J. Mod. Opt. **42**, 217–223 (1995).
23. M. F. Andersen, C. Ryu, P. Cladeé, V. Natarajan, A. Vaziri, K. Helmerson and W. D. Phillips, "Quantized rotation of atoms from photons with orbital angular momentum," Phys. Rev. Lett. **97**, 170406 (2006).
24. B. J. McMorran, A. Agrawal, I. M. Anderson, A. A. Herzing, H. J. Lezec, J. J. McClelland, and J. Unguris, "Electron vortex beams with high quanta of orbital angular momentum," Science **331** 192–195 (2011).
25. K. Saitoh and M. Uchida, "Electron beam carrying orbital angular momentum," Nihon Kessho Gakkaishi **58**, 79–84 (2016).
26. A. Yao and M. Padgett, "Orbital angular momentum: origins, behavior and applications," Adv. Opt. Photon. **3**, 161–204 (2011).
27. J. Nsofini, D. Sarenac, C. J. Wood, D. G. Cory, M. Arif, C. W. Clark, M. G. Huber, and D. A. Pushin, "Spin orbit states of neutron wavepackets," Phys. Rev. A **94**, 013605 (2016).
28. N. Voloch-Bloch, Y. Lereah, Y. Lilach, A. Gover and A. Arie, "Generation of electron Airy beams," Nature **494**, 331–335 (2013).
29. V. Grillo, E. Karimi, G. C. Gazzadi, S. Frabboni, M. R. Dennis and R. W. Boyd, "Generation of nondiffracting electron Bessel beams," Phys. Rev. X **4**, 011013 (2014).
30. I. A. Litvin, T. Mhlanga and A. Forbes, "Digital generation of shape-invariant Bessel-like beams," Opt. Express **23**, 7312–7319 (2015).
31. D. A. Pushin, D. G. Cory, M. Arif, D. L. Jacobson, and M. G. Huber, "Reciprocal space approaches to neutron imaging," Appl. Phys. Lett. **90**, 224104 (2007).
32. D. A. Pushin, M. Arif, D. L. Jacobson, C. K. Doe, and D. G. Cory, "Reciprocal space neutron imaging," Physica B **385–386**, 1402 (2006).
33. C. B. Shahi, M. Arif, D. G. Cory, T. Mineeva, J. Nsofini, D. Sarenac, C. J. Williams, M. G. Huber, and D. A. Pushin, "A new polarized neutron interferometry facility at the NCNR," Nuc. Inst. Meth. A **813**, 111–122 (2016).
34. M. Dietze, J. Felber and K. Raum, and C. Rausch, "Intensified CCDs as position sensitive neutron detectors," Nuc. Inst. Meth. A **377**, 320–324 (1996).
35. J. D. Fairweather, D. Spernjak, A. Z. Weber, D. Harvey, S. Wessel, D. S. Hussey, D. L. Jacobson, K. Artyushkova, R. Mukundan and R. L. Borup, "Effects of cathode corrosion on through-plane water transport in proton exchange membrane fuel cells," J. Electrochem. Soc. **160**, F980–F993 (2013).

1. Introduction

Holography was introduced by Dennis Gabor in 1948 [1], who showed that a far-field electron micrograph of an object could be used to make a transmission mask that allows the object to be reconstructed with visible light. Due to subsequent advances in the brightness of electron sources and, notably, the development of techniques for numerical reconstruction [2], holography has since become a significant branch of electron microscopy [3]. Atomic-resolution neutron holography has been demonstrated and applied to the determination of crystal structures [4–6]. The advent of coherent laser light sources in the 1960s made all–optical holography practical [7,8], to a degree that optical security holograms are now routinely printed on many paper currencies, credit cards, and identification documents [9, 10]. Holography remains a vibrant field of research in imaging science, as shown by numerous recent research papers [11–17].

Here we report the first demonstration of holography using neutron beams and macroscopic optical elements. Although deployed in a neutron interferometer (NI) with a Mach-Zehnder configuration [18], our method is a simple adaptation of the two-beam wedge technique introduced by Leith and Upatnieks [7, 8], and we discuss it using the conventional terminology of object, reference and reconstruction beams.

Our object is a spiral phase plate (SPP) that we previously used to impart orbital angular

Optics EXPRESS

momentum (OAM) to neutron waves [19]. In this respect our experiment is a neutron analogue of the holography of braided optical fibers performed by Bazhenov, Vasnetsov and Soskin [20]. Our neutron holograms resemble the fork dislocation gratings synthesized by them and by Heckenberg, *et al.* [22], which have since been used to transfer angular momentum to small particles, [21] atoms, [23], electrons [24, 25] and light [26]. Digital reconstruction of this hologram provides information about the phase generated by the SPP, which should be useful in the design of the next generation of neutron OAM experiments [27].

Holography provides a direct connection between the refractive and diffractive mechanism of OAM imprinting of particles and waves. This first demonstration of neutron holography of a macroscopic object suggests that the complex grating methods used to produce OAM, Bessel, and Airy beams for light and electrons [28–30] may also be extended to neutrons.

2. Schematic of neutron holography

We use a NI to effect the coherent superposition of an object beam and a reference beam. As shown in Fig. 1(b), our object beam consists of neutrons that have passed through an aluminum SPP in one arm of the NI. The SPP imprints a spatially-varying phase of $q\phi$ upon the neutron input beam, where q is the topological charge of the SPP [27] and ϕ is the azimuthal angular coordinate on the neutron wavefront, with coordinate origin being the center of the SPP surface. The other arm of the NI provides the reference beam. The holographic image is constructed from the interferogram of object and reference beams, as recorded by a neutron sensitive digital camera. When no optical device is present in the reference arm, this interferogram displays the topological charge of the object beam, which is the same as that of a beam with orbital angular momentum (OAM) of $\ell\hbar$, where $\ell = q$ [19]. By placing a prism into the reference beam we introduce a linear gradient which effectively tilts the wavefronts [31, 32].

The experiment is an expectation valued measurement over many events, each of which involves only a single neutron. In optics one would manipulate fully coherent beams and in the neutron case where an interferometer is used the coherence need only be larger than the deviation due to the prism and the object. There is no advantage in the neutron case in having the coherence beyond that because there is one neutron at a time in the interferometer and the hologram is built up from an incoherent superposition of many events. The neutron coherence length is a function of the beam momentum spread, and in our experimental setup it is on the order of microns, while the incident neutron beam is several millimeters in size, and the deviation due to the SPP and the prisms is on the order of nanometers. Hence the coherence length we use captures the physics needed to perform holography. We have combined neutron interferometery with holography and an appropriate coherence length must be used as the modification of the neutron coherence is extremely difficult and time consuming [18].

The transverse wavefunction of the incoming neutron wavepacket, which is centered at an arbitrary position (x_0, y_0) in the beam, can be taken to be:

$$\Psi_t = (2\pi\sigma^2)^{-1/2} e^{-\frac{(x-x_0)^2+(y-y_0)^2}{4\sigma^2}}, \tag{1}$$

where $\sigma_x = \sigma_y \equiv \sigma$ is the coherence length. After the first NI blade there is a coherent superposition of the two paths inside the interferometer. The wavefunction of the object beam (Ψ_o) acquires a $e^{-iq\phi}$ term due to the SPP and the wavefunction of the reference beam (Ψ_r) acquires a e^{-iky} term due to the prism; where k is proportional to the spatial gradient due to the prism, and y is the vertical coordinate in the plane of the image, as indicated in Fig. 1(b). In addition, there is an intrinsic phase θ between the two paths. The last NI blade coherently combines the two paths and the intensity at the camera is then given by:

Optics EXPRESS

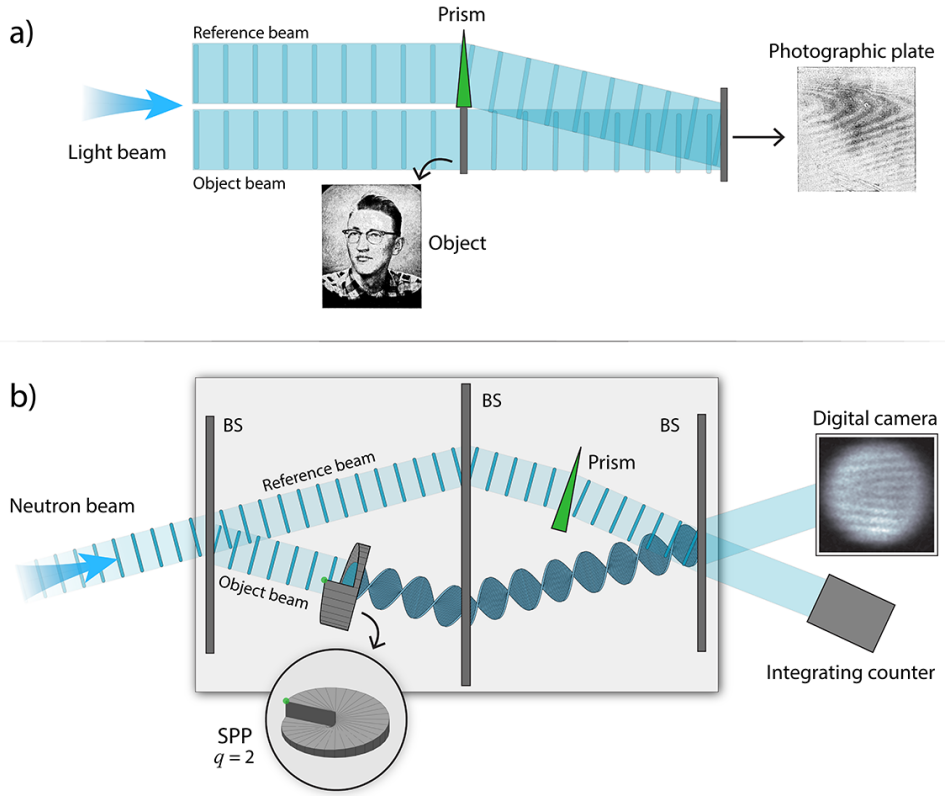

Fig. 1. (a) The off-axis method of optical holography of semitransparent objects introduced by Leith and Upatnieks. The object here is a continuous-tone transparency; its hologram was recorded on a photographic plate. Redrawn from figures of [8]: the object shown here is actually the holographic reconstruction of the original object, said to be a good facsimile of the original. (b) An artistic depiction of the neutron holography experiment. A neutron enters a single-crystal silicon Mach-Zehnder neutron interferometer (NI) and is separated into two paths by the left beamsplitter (BS). A spiral phase plate (SPP) with q = 2 is placed in the lower path, generating the object beam; a prism tilts the wavefront of the upper path to provide the reference beam. Object and reference beams are reflected at the central BS, and are coherently combined at the right BS. One of the output beams of the right BS is sent to an imaging detector, the other to an integrating counter that serves as an intensity monitor. Note that the experiment is an expectation valued measurement over many events, each of which involves only a single neutron. That is, there is one neutron at a time in the NI and the hologram is build up from an incoherent superposition of many events.

$$I = \int_0^d \int_0^d |\Psi_r + \Psi_o|^2 dx_0 dy_0 = A + B\cos(ky - q\phi + \theta), \tag{2}$$

where d is the beam size, and $d >> \sigma$; and A and B are experimental constants which are ideally equal to $1/2$. The intensity profile is equivalent to what is obtained with a fully coherent beam [22]. Figure 2(a) displays the calculated interferograms when only the SPP is present in the NI, and Fig. 2(b) shows the interferograms when both the SPP and the prism are present. The embedded video (Visualization 1) shows the data of Fig. 2(b) as a continuous function of the

Optics EXPRESS

topological charge q. We complete the holographic process by applying digital reconstructions to the measured forked dislocation structures, showing that they yield the phase and intensity profiles associated with the SPP.

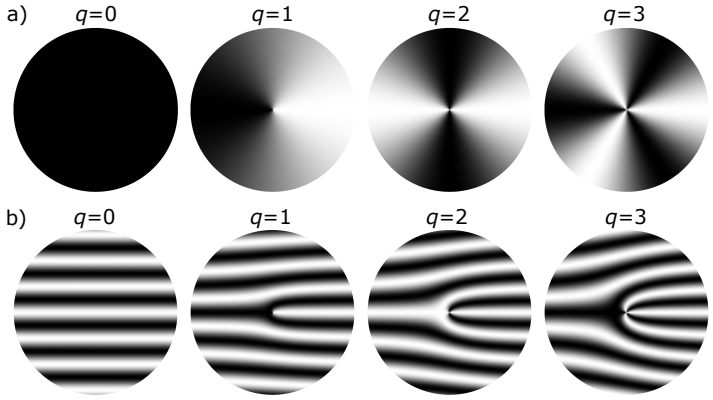

Fig. 2. Simulation of the intensity profiles at the 2D detector for SPPs with topological charges of $q = 0, 1, 2, 3$ in the object beam, and (a) no prism in the reference beam, and (b) a prism in the reference beam. The linked video (Visualization 1) shows the intensity profile as a continuous function of the topological charge q. Fractional values of q correspond to admixtures of orbital angular momentum states with various integer values of ℓ. Note that the successive fork dislocations unfold as q passes through integer values.

3. Experimental method

The experiment was performed at the Neutron Interferometry and Optics Facility (NIOF) at the National Institute of Standards and Technology (NIST) Center for Neutron Research (NCNR) [33]. Neutrons generated by a 20 MW nuclear research reactor are cooled via a liquid hydrogen moderator, and pass through a system of beamlines to experimental stations. A monochromator at the NIOF beamline is used to select neutrons with energies around 11 meV, corresponding to a de Broglie wavelength of $\lambda_{\mathrm{dB}} = 0.271$ nm. This cold neutron beam is incident on the NI, which is an example of the devices discussed in [18, 33]. The NI was made using a single ingot of silicon machined so that it has three blades supported by a common base. The common base insures sub-arcsecond alignment between the crystal blades. Neutrons entering the interferometer are Bragg diffracted by the (111) lattice planes of the crystal blades forming two spatially separate paths. Phase differences between these two paths cause interference in the last blade of the interferometer. This interference is then detected using either a fully integrating ^{3}He proportional counter or a neutron-sensitive imaging camera.

An aluminum SPP with $q = 2$ was placed in the object beam. The construction of the SPP is described by Clark, *et al.* [19]. We note here that the SPP was made with a standard milling machine cutting a spiral staircase into the surface of a segment of aluminum dowel. A topological charge $q = 2$ is obtained with a staircase with a total vertical descent of 224 μm, which is $\approx 10^6 \times \lambda_{\mathrm{dB}}$. Those experienced in optical design for visible light may find it surprising that the mechanical figure of an optical component need only be controlled within a few thousand multiples of the operational wavelength. This is possible with neutrons, since neutron indices of refraction for most materials differ from unity by a few parts per million.

In the reference beam a vertical linear gradient was introduced by using two identical fused silica optical wedges [31] arranged back-to-back. These wedges had a 6° angle and each could be rotated independently a full rotation of 2π. Note that any non-gradient phase shift inside the interferometer would only shift the pattern at the camera.

Optics EXPRESS

In our experiments, the integrating counter was used to measure the average rate of neutrons exiting the interferometer, which was about $r = 20\ \mathrm{s}^{-1}$. This rate determines an average time interval $\tau = 1/r = 50$ ms between detection of successive neutrons. Since the distance of the NI from the reactor is 30 m, and the neutron velocity is 1,460 m/s it takes 20 ms for a neutron to travel from the reactor to the NI. Thus, just after one neutron has been detected, the next neutron to be detected has not yet been produced by the reactor. The interference fringes that are seen in our data are truly those of neutrons interfering with themselves.

For the images depicted in Fig. 3, the wedges were adjusted to give a theoretical linear phase gradient of 3.4 rad/mm. Reactor fluctuations were monitored using the ^{3}He detector. The interferograms were recorded on a neutron-sensitive digital camera [6] that has an active area of 25 mm diameter and a spatial resolution of 100 μm [34]. The neutron quantum efficiency of the camera is 18 % and individual images were taken in 28-hour runs. The average of three images was used for analysis.

4. Results

Figure 3 depicts interferograms for four different configurations. Figure 3(a) shows the grayscale intensity profile obtained with an empty interferometer. It can be seen that the input beam is nonuniform. Figure 3(b) shows the experimental and simulated interferograms for the case in which only the prism is placed in the reference beam of the interferometer. The number of fringes in the simulated interferogram are in agreement with the measured image. Figure 3(c) shows the interferogram when only the SPP is present in the object beam. It is necessary to add a horizontal gradient of 0.3 rad/mm to the simulation for Figs. 3(a) and 3(b) to reproduce the measured figures. This horizontal gradient might explain the nonuniformity of Fig. 3(a) as well. Figure 3(d) shows the hologram obtained when the prism is placed in the reference beam and the SPP is placed in the object beam. The expected fork grating pattern is recognizable in this hologram.

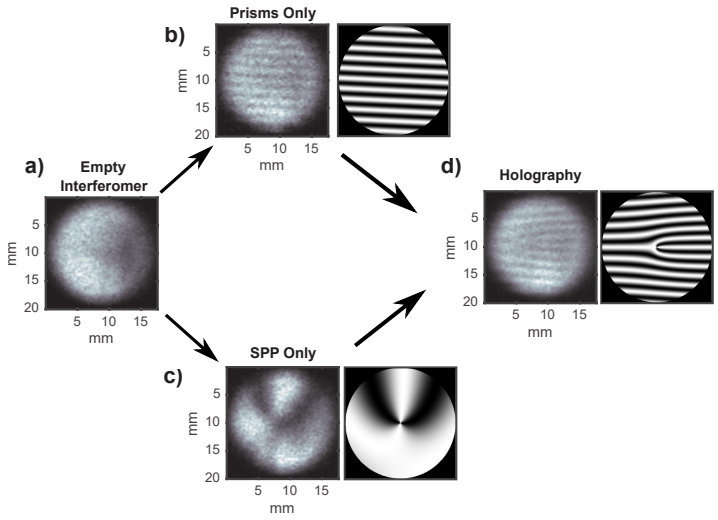

Fig. 3. Measured and simulated interferograms at the 2D detectors for the $q = 2$ SPP and 6° fused silica prism independently, as well as when both are placed in the neutron interferometer to produce the pitch fork pattern. It is necessary to add a horizontal gradient of 0.3 rad/mm to the simulation to reproduce the measured images.

Figure 4 shows the numerical reconstruction [2] of the experimental images shown in Figs. 3(b) and 3(d). The reconstruction was obtained by computing the Fresnel-Kirchhoff diffraction integral in the Fresnel limit for $\lambda d = 70\ \mathrm{mm}^2$ using the expression:

Optics EXPRESS

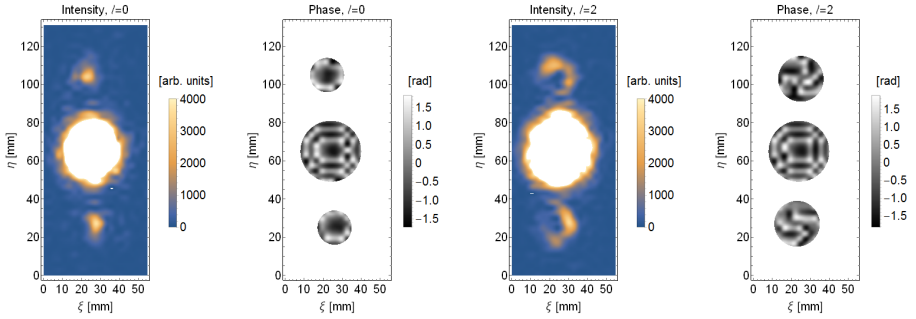

Fig. 4. Intensity and phase profiles of the computed hologram reconstruction for the measured images in Fig. 3(b) corresponding to no SPP in the object beam; and Fig. 3(d) corresponding to a $q = 2$ SPP being in the object beam. Note that the phase range is from $-\pi/2$ to $\pi/2$, which is why we see four arms instead of two as seen on Fig. 2(a), where the range is from $-\pi$ to π. The images are interpolated, and show the central 20x48 array of the numerical reconstruction. The mask for the phase plots is included for clarity. The linked video (Visualization 2) shows the two-dimensional intensity as a continuous function of the parameter λd, and the linked video (Visualization 3) shows the phase profile with the overall phase in the reconstruction plane varied.

$$\Gamma(\nu,\mu) = \frac{i}{\lambda d} e^{-i\pi\lambda d(\nu^2+\mu^2)} \mathcal{F}\left\{h(x,y)\exp\left(-i\frac{\pi}{\lambda d}(x^2+y^2)\right)\right\} \tag{3}$$

where λ is the wavelength of the virtual wave illuminating the hologram; d is the distance between the hologram and the reconstruction plane; $\mathcal{F}$ is the Fourier transform; x and y are the hologram coordinates; $h(x,y)$ is the obtained hologram image; and ν and μ are the normalized forms of image reconstruction coordinates (ξ,η), such that $(\nu,\mu) = (\xi,\eta)/(\lambda d)$. The Fourier transform was computed using the Fast Fourier Transform algorithm. The reconstructed intensity, $|\Gamma|^2$, and the phase, $\tan^{-1}(\mathrm{Im}[\Gamma]/\mathrm{Re}[\Gamma])$, were then computed.

For the hologram, it can be seen from the uniform intensity distribution that the zero diffraction order corresponds to $\ell = 0$, while the first diffraction order displays the doughnut profile indicative of a beam carrying OAM. By plotting the reconstructed phase we confirm that the first diffraction beams correspond to beams with $\ell = 2$ as expected. Note that the spherical phase outside the Fourier transform was dropped in the Eqn. (3) reconstruction integral in order to look down the diffracted OAM beam paths and not along the reconstruction plane normal. The two linked videos show the two-dimensional intensity with the variable λd increasing with time (Visualization 2) and the phase profile as a function of the overall phase in the reconstruction plane (Visualization 3). As the value of λd increases, we see the formation of first-order diffraction peaks with doughnut-shaped intensity profiles, corresponding to orbital angular momentum $\ell = 2$.

5. Conclusion

Using a neutron interferometer, we have for the first time demonstrated digitally recorded neutron holography of a macroscopic object: a spiral phase plate. Numerical reconstruction of the recorded hologram reveals the variation of neutron phase over the surface of that plate. This method provides a new tool for interferometric testing of neutron optics and the characterization of coherence of neutron beams. It offers an extension of coherent phase control techniques to applications in neutron radiography and imaging, which are uniquely useful in the analysis of buried interfaces [6, 35].

Optics EXPRESS

Funding

Canadian Excellence Research Chairs (CERC) (215284); Natural Sciences and Engineering Research Council of Canada (NSERC) Discovery (RGPIN-418579); Collaborative Research and Training Experience (CREATE) (414061); National Science Foundation (NSF) (PHY-1205342,PHY-1307426); U.S. Department of Energy (DOE) (DE-FG02-97ER41042); National Institute of Standards and Technology (NIST) Quantum Information Program.

Acknowledgments

We thank Sean Kelley for his contributions to the figures.